ELSEVIER

Contents lists available at ScienceDirect

Combustion and Flame

journal homepage: www.elsevier.com/locate/combustflame



An experimental investigation of flame and autoignition behavior of propane



Miles A. Burnett^{a,*}, Margaret S. Wooldridge^{a,b}

- ^a Department of Mechanical Engineering, University of Michigan, Ann Arbor, MI 48109, United States
- ^b Department of Aerospace Engineering, University of Michigan, Ann Arbor, MI 48109, United States

ARTICLE INFO

Article history:
Received 15 September 2020
Revised 1 December 2020
Accepted 2 December 2020
Available online 18 December 2020

Keywords: Propane Autoignition Rapid compression facility

ABSTRACT

Autoignition delay time data are one important means to develop, quantify, and validate fundamental understanding of combustion chemistry at low temperatures (T<1200 K). However, low-temperature chemistry often has higher uncertainties and scatter in the experimental data compared with high-temperature ignition data (T>1200 K). In this study, autoignition properties of propane and oxygen mixtures were investigated using the University of Michigan rapid compression facility in order to understand the effects of ignition regimes on low-temperature ignition data. For the first time for propane, autoignition delay times were determined from pressure histories, and autoignition characteristics were simultaneously recorded using high-speed imaging of the test section through a transparent end-wall. Propane mixtures with fuel-to- O_2 equivalence ratios of $\phi=0.25$ and $\phi=0.5$ and O_2 -to-inert gas molar ratios of 1:3.76 were studied over the pressure range of 8.9 to 11.3 atm and the temperature range of 930 - 1070 K. The results showed homogeneous or strong autoignition occurred for all $\phi = 0.25$ experiments, and inhomogeneous or mixed autoignition occurred for all $\phi = 0.5$ experiments. While a limited temperature range is covered in the study, importantly the data span predicted transitions in autoignition behavior, allowing validation of autoignition regime hypotheses. Specifically, the results agree well with strong-autoignition limits proposed based on the Sankaran Criterion. The autoignition delay time data at the strong-ignition conditions are in excellent agreement with predictions using a well-validated detailed reaction mechanism from the literature and a zero-dimensional modeling assumption. However, the experimental data at the mixed autoignition conditions were systematically faster than the model predictions, particularly at lower temperatures (T < -970 K). The results are an important addition to the growing body of data in the literature that show mixed autoignition phenomena are important sources of the higher scatter observed in the low-temperature autoignition data for propane and other fuels. The results are discussed in terms of different methods to capture the effects of pre-autoignition heat release associated with mixed autoignition conditions and thereby address some of the discrepancies between kinetic modeling and experimental measurements.

© 2020 The Combustion Institute. Published by Elsevier Inc. All rights reserved.

1. Introduction

Due to the prevalence of propane in natural gas blends, the fundamental chemical structure of propane, and the importance of propane as a primary fuel and intermediate in combustion chemistry, many experimental studies on the autoignition behavior of propane are available in the literature. As outlined in Goyal et al. [1] and Samini-Abianeh et al. [2], the available data span many different experimental facilities, including shock tubes [3–12], rapid compression machines (RCMs) [9,13,14], flow reactors [15–18], and

* Corresponding author.

E-mail address: maburn@umich.edu (M.A. Burnett).

jet stirred reactors [19]. The diversity of experimental approaches has allowed propane combustion data to be collected over a large range of temperatures, pressures, concentrations, and equivalence ratios. Much of the autoignition delay time data for propane comes from high-temperature studies conducted using shock tubes, and the data are generally in good agreement and exhibit relatively low scatter at higher temperatures (e.g., autoignition delay times are within a factor of 2 at temperatures above 1300 K), as seen in the Arrhenius diagram presented in Fig. 1. The data in Fig. 1 are for fuel-to-air equivalence ratios of 0.5 (molar basis) and have been normalized by pressure to 10 atm. However, the scatter in the data increases remarkably at lower temperatures, e.g., with over an order of magnitude variation in autoignition delay time at temperatures below 900 K. Unscaled data for the studies cited in

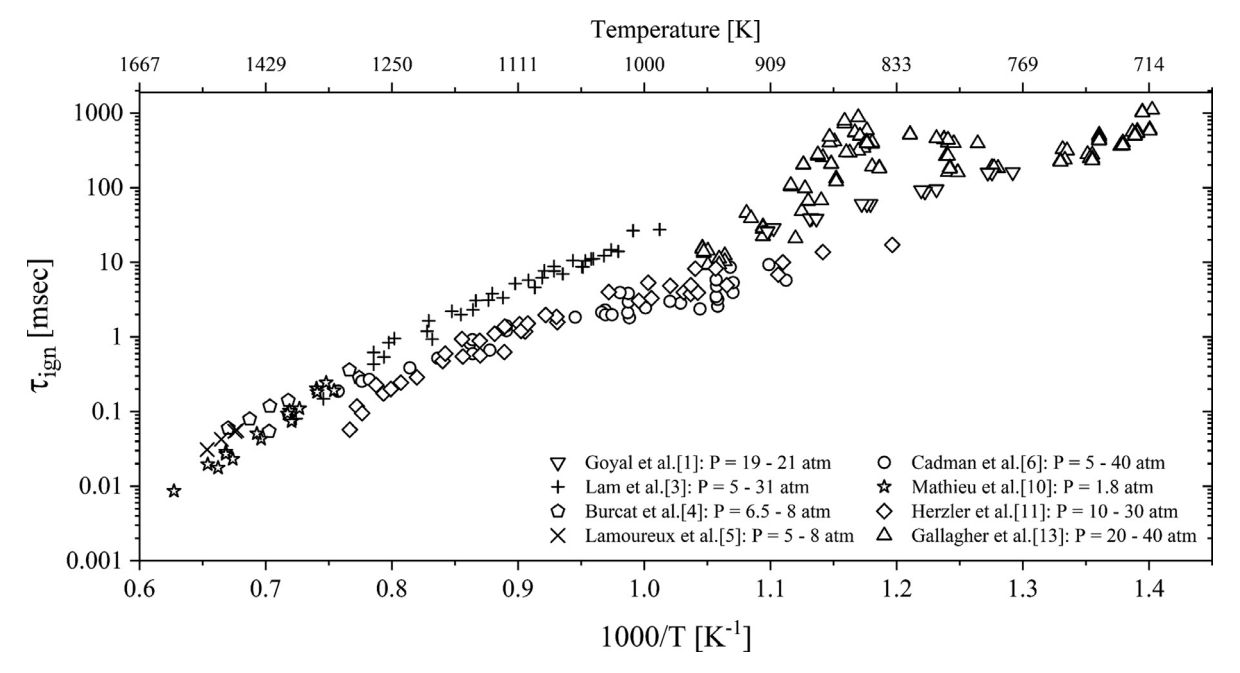


Fig. 1. Summary of autoignition delay time data for propane/air mixtures at ϕ =0.5. The data have been normalized to P = 10 atm using scaling of $\tau_{\rm ign} \propto 1/P$. Unscaled data and autoignition delay time results for other equivalence ratios are provided in the Supplemental Material.

Fig. 1, and autoignition delay time results for other equivalence ratios are provided in the Supplemental Material. Low-temperature autoignition behavior of propane is particularly of interest because propane is the smallest alkane to exhibit negative temperature coefficient (NTC) behavior at lower temperatures (i.e., below 1000 K) [1,13,20,21], and lower temperature combustion strategies are promising means to increase efficiency and reduce emissions in transportation and stationary power generation applications [22-24]. However, there are challenges to lower temperature combustion strategies including misfire and reduced control over heat release and reaction rates [22,23]. Accurate understanding of lowtemperature combustion characteristics is important for successfully advancing these high-efficiency, low-emissions applications, and autoignition delay time data are one important means to develop, quantify, and validate fundamental understanding of combustion at low temperatures.

The specific focus of the present work is on the interaction between volumetric autoignition and reaction fronts that is more likely to affect autoignition data at lower temperatures [25-30]. The presence of reaction fronts is attributable to the thermal gradients that are ubiquitous to all experimental facilities. Thermal gradients are created (in part) by mixing induced by the compression process in rapid compression machines and by non-ideal shock behavior and boundary layer effects in shock tubes. The interaction between autoignition and reaction fronts leads to autoignition behavior typically referred to as weak, mild or mixed autoignition [25-28,31] and has been studied in shock tubes [32-37] and RCMs [25,26,28]. In particular, earlier work that included high-speed imaging has provided key insights connecting the effects of reaction fronts and autoignition phenomena on autoignition delay time data [25,26,28,34]. Since pre-ignition pressure rise can be associated with volumetric kinetics (e.g., [38]), the use of high-speed imaging coupled with pressure data to characterize ignition behavior is vital to distinguish between volumetric lowtemperature heat release and mixed, mild or weak ignition. The presence of reaction fronts can dramatically accelerate autoignition delay times as notably observed with syngas autoignition at low temperatures [26] or have limited to no effect on autoignition delay times [29], depending on the autoignition regime [25–27].

Many studies have documented the characteristics of the different autoignition regimes, and these works have provided researchers with the important data to advance theories on the state and mixture conditions leading to different autoignition behavior (see Zeldovich [39], Sankaran et al. [40], Bansal and Im [30], Im et al. [41], and references therein). To briefly summarize the characteristics of the autoignition regimes, strong autoignition is when autoignition chemistry dominates, and the entire test gas mixture autoignites simultaneously and homogeneously, i.e., without spatial variation. Strong autoignition is characterized by a rapid increase in pressure, and autoignition delay times that are highly repeatable with low experimental uncertainties. Weak, mild or mixed autoignition occurs when reaction fronts propagate from one or more localized sites within the reaction chamber while the remainder of the unburned mixture is simultaneously undergoing autoignition. The pressure rise associated with the heat release from the reaction fronts compresses the unburned gases in the combustion chamber, typically accelerating the autoignition chemistry and leading to homogeneous autoignition of the remaining unburned gases. Mansfield and Wooldridge [26] defined this behavior as "mixed" autoignition due to the presence of both inhomogeneous characteristics (e.g., the presence of reaction fronts) and eventual homogeneous autoignition of the unburned gas region. There have been many different means of defining strong autoignition in the literature, including Meyer and Oppenheim [31] who classified strong autoignition solely by whether a transition to detonation occurred. However, most of the recent studies have defined strong autoignition as spatially uniform autoignition behavior with the absence of localized reaction fronts prior to autoignition.

Understanding the different types of autoignition phenomena is critical to building confidence in the autoignition delay time data used for developing and validating combustion chemistry. In particular, most models used to test combustion reaction mechanisms represent autoignition experiments of shock tubes and RCMs as zero-dimensional, i.e., they do not include spatial effects. The assumption of uniform state conditions is invalid for mixed autoignition regimes and can lead to incorrect conclusions when comparing experimental and modeling data. Thus, theory that can predict

a priori when mixed autoignition can affect autoignition delay time data is key to understanding experimental uncertainties and limitations. Additionally, it is valuable if the theory is accessible to a broad range of combustion researchers without the need for extensive estimates, measurements, and simulations. The theory that is the focus of the present work is the autoignition criterion proposed by Sankaran et al. [40], which in turn was based on work by Zeldovich [39] that compares the laminar flame speed of a given mixture to the reaction front propagation rate driven by the thermal gradients present in the physical system. There are several ignition criteria that have been proposed in recent years, including works by Im et al. [41] and Grogan et al. [42]. The fairly simple inequality, referred to as the Sankaran Criterion, is a prediction of the location of the strong autoignition limit based on comparison of the homogeneous chemical reactivity of a mixture with the deflagration flame speed of the mixture. The Sankaran Criterion is captured within the theory proposed by Im et al. [41] and Grogan et al. [42], but the latter theories include turbulent mixing scales. Turbulent mixing scales have not been measured in the UM-RCF and would therefore be a source of high uncertainties, hence they are not utilized in the present work. Additionally, the Sankaran criterion is considered more accessible to combustion engineers, because it is based on more easily and more often measured input parameters of temperature and pressure.

The Sankaran Criterion can be used to make a priori predictions of autoignition behavior, and the validity of the Sankaran Criterion as a predictive tool was demonstrated by Mansfield and Wooldridge [26] for syngas (CO and H₂) and by Mansfield et al. [25] for iso-octane. The theory was further developed and non-dimensionalized in the work by Im et al. [41]. Prior studies indicate the Sankaran Criterion is not fuel specific; however, additional demonstrations of the theory for other fuels, particularly for fundamental alkanes like propane, are important to building confidence in the validity of the theory. Additionally, mixed autoignition is often associated with lower temperatures (T < 1200 K), where experimental measurements frequently exhibit higher scatter (e.g., see Fig. 1) and larger discrepancies with model predictions (e.g., syngas [26]) compared with higher temperature experiments. Thus, the objectives of the present work were to test the Sankaran Criterion for application to propane autoignition, providing further evidence of its utility as a general a priori method for accurately predicting autoignition behavior, to evaluate the existing propane autoignition data in the literature in the context of the Sankaran Criterion, and to consider simplified means to account for mixed ignition phenomena when comparing experimental data with model predictions. This work presents the first study of ignition regimes for a straight chain alkane, and successful demonstration of the approach for interpreting data in the literature has broad implications on low-temperature autoignition data of other fuels.

2. Methods

2.1. Experimental

The UM-RCF is a uniquely designed experimental apparatus that can create uniform state conditions at high temperatures (600–2000 K) and high pressures (1–40 atm) using a free piston (sabot) to isentropically compress a test gas mixture. While these temperatures and pressures are achievable with the UM-RCF, limits are further imposed by the test times for propane autoignition at the mixture compositions and state conditions studied. Test times greater than 75 ms can be affected by considerable heat losses that impact ignition, and test times less than 1 ms are convolved with the compression process. Thus, the current work targeted state and mixture conditions between the limits of test times from 1 to 75 ms. A detailed description of the UM-RCF, including dimen-

sions, components, and characterization of its performance, can be found in Donovan et al. [43] and He et al. [44]. Briefly, the UM-RCF consists of two long cylinders that are the driver and driven sections. The sections are separated by a fast globe valve and a sheet of Mylar film that divides the two sections until the start of an experiment. The test section is a small, cylindrically-shaped volume that is ~50 mm in both length and diameter and is located at the downstream end of the driven section.

The test gas mixtures are prepared in a stainless-steel mixing tank with an automatic stirring mechanism, with mixture composition determined through relative partial pressure measurements of each gas component. The mixture is typically left to stir overnight to ensure homogeneous composition. The component gases used in this study were propane (PurityPlus, >99.5%), nitrogen (PurityPlus, >99.999%), argon (PurityPlus, >99.999%) and carbon dioxide (PurityPlus, >99.995%). Mixture uncertainty is predominantly a result of the uncertainty in the pressure transducers used to calculate mixture composition. Overall, uncertainty is < 0.1% for fuel concentration and < 0.05% for oxygen and diluent concentration.

Before each autoignition experiment, a vacuum pump is used to evacuate the driven section, which is subsequently filled with the prepared test gas mixture. The driver section is then filled with compressed air that is used to propel the sabot down the length of the driven section upon opening the globe valve. The process rapidly compresses the test gas mixture into the test section located on the opposite end of the driven section, with the bulk of the compression occurring in the last 10 ms of the compression stroke. At the end of compression, the sabot seats via an annular interference fit that seals the test gas mixture within the test section at the desired thermodynamic conditions.

Pressure time-history measurements are obtained in the test section before, during, and after the compression process using a pressure transducer (Kistler 4045A2) and charge amplifier (Kistler 4618A0) with a 100 kHz sampling frequency. The pressure measurements have an uncertainty of \leq 1% (~0.1 atm). A transparent polycarbonate end-wall is used for optical access for high-speed imaging of the autoignition process. Images for this study were recorded using a CMOS camera (Phantom V711-32G-MAG-C, 512 \times 512 pixels) with a 50 mm lens (Navitar, F0.95), a 62 mm lens (HOYA +2 Zoom), and a 62 mm UV(0) filter (Hoya). The video sequences were recorded at 25,000 frames per second with 39.6 μ s exposure time.

For this study, the UM-RCF was used to conduct autoignition experiments for mixtures of propane and oxygen with fuel-to-O₂ equivalence ratios of $\phi = 0.25$ and $\phi = 0.5$ with air levels of dilution; meaning the molar O₂-to-diluent gas ratio was 1:3.76. Three diluent gases (N2, Ar, and CO2) were used, with N2 being the primary diluent gas, and the levels of Ar and CO2 were adjusted to control the end-of-compression test gas temperature. Experiments with an equivalence ratio of $\phi = 0.25$ included end-ofcompression temperatures between 930 and 1070 K and pressures between 8.9 and 10.4 atm, and experiments with an equivalence ratio of $\phi = 0.5$ included end-of-compression temperatures between 945 and 1010 K and pressures between 9.7 and 11.3 atm. As noted earlier, these conditions place the autoignition delay times between 1 and 75 ms. Test times >75 ms are significantly affected by heat losses in RCMs, shock tubes and other devices, increasing measured autoignition delay times beyond the effects of only chemical kinetics. Test times less than 1 ms are convolved with the compression process with many RCMs, and shock tubes and other experimental approaches may yield lower uncertainties. While a limited temperature range is covered in the study, importantly the data span predicted transitions in autoignition behavior, allowing validation of the autoignition regime hypothesis. The mixture composition and thermodynamic state conditions for each experiment are summarized in Table S1 in the Supplemental Material.

2.2. Computational

Predictions for autoignition delay times were made using the Healy et al. C1-C5 chemical kinetic mechanism [45] with the Chemkin [46] program suite (version 19.1, x64) for a zerodimensional, closed homogeneous reactor model with constant total volume and constant total energy. The original reaction mechanism by Healy et al. [45] was used with no changes to any of the rate coefficients. The predictions were obtained using the mixture composition and thermodynamic state (T and P) from each experiment as the initial conditions for the simulations. There are many different methods for quantifying uncertainties due to the reaction chemistry used with Chemkin simulations. Details on the uncertainty quantification for the simulations are provided in the Supplemental Material along with results of time-dependent sensitivity analysis. The effects of different modeling assumptions were also evaluated, including simulating the compression stroke. Comparison of the modeling approaches is provided in the Supplemental Material. Differences in the predicted autoignition delay times due to different modeling approaches were less than the uncertainty associated with the elementary chemistry of the reaction mechanism. Therefore, constant volume and constant energy modeling was used throughout this work, and the error bars represented in figures are due to uncertainties in the rate coefficients used in the reaction mechanism. Note that quantifying uncertainties in reaction mechanisms remains non-standardized in the combustion community. Systematic methods for representing modeling uncertainties when reaction chemistry is significant (as in autoignition modeling) is an important area for future work.

The strong autoignition limit was calculated using the Sankaran Criterion as described in Sankaran et al. [40] and as applied in Mansfield and Wooldridge [26] and Mansfield et al. [25]. As described by Sankaran et al. [40], the Criterion compares the relative magnitude of spontaneous propagation of autoignition and deflagration, as per Eq. (1):

$$\left| \frac{d\tau}{dT} * \frac{dT}{dx} \right| > \left(s_u^0 \right)^{-1} \tag{1}$$

where the gradient of the autoignition delay time $(\mathrm{d}\tau/\mathrm{d}x)$ is decomposed into the product of the thermal gradient of the physical system $(\mathrm{d}T/\mathrm{d}x)$ and the thermal sensitivity of the autoignition delay time $(\mathrm{d}\tau/\mathrm{d}T)$, and s_u^0 is the laminar flame speed. When spontaneous propagation dominates the autoignition behavior of the combustion system and the thermal gradients are small, homogeneous or strong autoignition is expected, and the inequality is true. When deflagration dominates and laminar flames consume the fuel faster than the autoignition chemistry, inhomogeneous or weak autoignition is expected, and the inequality is false. Between the limiting strong and weak autoignition regimes, mixed autoignition is expected with some attributes of autoignition and propagation of local reaction fronts.

To evaluate Eq. (1), autoignition delay times were systematically calculated over a broad range of thermodynamic conditions for $\phi=0.25$ and $\phi=0.5$. The results were used to calculate the thermal sensitivity of the autoignition delay time, $\mathrm{d}\tau/\mathrm{d}T$ for each equivalence ratio. A constant thermal gradient of 5 K/mm value was applied in Mansfield and Wooldridge [26] and Mansfield et al. [25] for syngas and *iso* octane, respectively. The value of 5 K/mm originates from temperature measurements made in the UM-RCF by Donovan et al. [43]. Laminar flame speeds were calculated using the Premixed Laminar Flame-Speed Calculation in Chemkin [46] with the Healy et al. [45] reaction mechanism, thermodynamic data and transport data. Laminar flame speeds for temper-

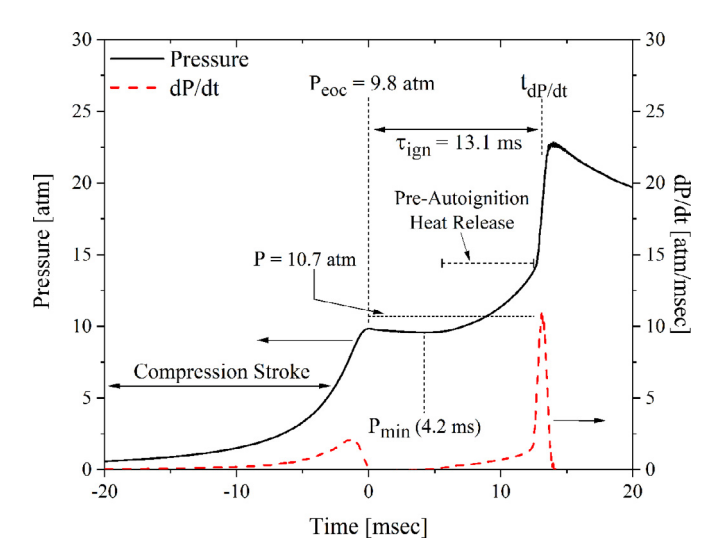


Fig. 2. Typical experimental pressure history exhibiting characteristics of mixed autoignition for conditions of P=10.7 atm, T=963 K, and $\phi=0.5$ with a mixture composition of 2.06% C₃H₈/20.60% O₂/77.34% N₂. $P_{\rm eoc}$ is the pressure at the end of the mechanical compression stroke, and P is the time-averaged pressure from $P_{\rm eoc}$ to P at maximum dP/dt.

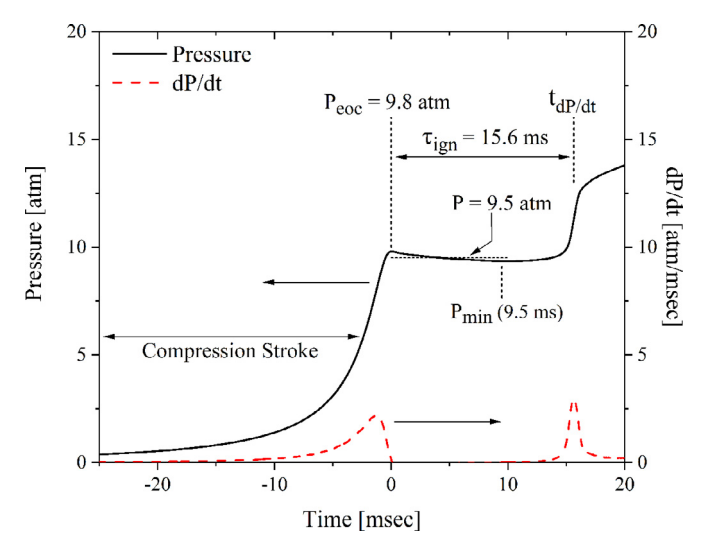


Fig. 3. Typical experimental pressure history exhibiting characteristics of strong autoignition for experimental conditions of P=9.5 atm, T=990 K, and $\phi=0.25$ with a mixture composition of 1.04% $C_3H_8/20.80\%$ $O_2/78.16\%$ N_2 . P_{eoc} is the end of the mechanical compression stroke, and P is the time averaged pressure from P_{eoc} to P at maximum dP/dt.

atures above ~1000 K and below ~750 K were extrapolated from calculations at intermediate temperatures using an exponential fit.

3. Results and discussion

Pressure time histories and high-speed video were recorded for each experiment. The pressure data were used to determine the autoignition delay time for each experiment, and the high-speed videos were used to observe and classify the autoignition behavior based on the chemiluminescence observed. Typical pressure histories for inhomogeneous (mixed) and homogeneous (strong) autoignition are presented in Figs. 2 and 3, respectively. For both experiments, the pressure data show the compression stroke causes a smooth increase in pressure in the test section until the end of compression. After the end of compression, there is a slight pressure decrease in both experiments caused by heat transfer from the test gas to the cooler test-section walls. P_{\min} is

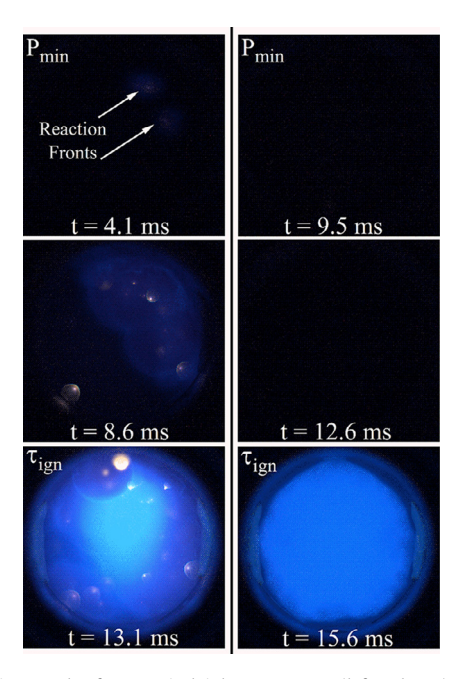


Fig. 4. Imaging results from typical inhomogeneous (left column) and homogeneous (right column) autoignition experiments. The images in the left column are from the same experiment as the data presented in Fig. 2. The images in the right column are from the same experiment as the data presented in Fig. 3. Note the presence and propagation of reaction fronts at the inhomogeneous autoignition conditions.

the minimum pressure after the end of compression and is labeled in the figures. The key difference in the two pressure histories is near the time of autoignition. The pressure history for the mixed (inhomogeneous) autoignition experiment in Fig. 2 shows a gradual pressure rise starting around P_{\min} (from $t=\sim5$ to 12 ms), prior to the rapid increase in pressure due to autoignition at t=13.1 ms. This pre-autoignition heat release is most apparent in the pressure derivative data, also presented in Fig. 2. The pressure history for the strong (homogeneous) autoignition experiment in Fig. 3 shows no heat release prior to autoignition at 15.6 ms.

Figure 4 presents imaging results corresponding to the experimental data presented in Figs. 2 and 3. The images in the left column of Fig. 4 exhibit inhomogeneous characteristics and are from the same experiment as the pressure data presented in Fig. 2. The images in the right column of Fig. 4 exhibit uniform or homogenous autoignition characteristics and are from the same experiment as the pressure data presented in Fig. 3. The three still images from each experiment are all from after the end of compression and correspond to times at: 1. P_{\min} , 2. an intermediate time, and 3. the time of autoignition. Comparison of the pressure and imaging data from the inhomogeneous experiment (i.e., Fig. 2 and the left column of Fig. 4) shows the gradual pressure rise before autoignition corresponds with the propagation of reaction fronts in the test section (t = 4 to ~13 ms), and the rapid pressure rise at 13.1 ms corresponds with autoignition of the reactants not consumed by the reaction fronts. The timing of the first observation of the reaction fronts (t = -4 ms) is consistent with the timing of the first observation of an increase in the rate of pressure rise after the end of mechanical compression of the test gas mixture ($t=\sim 5$ ms). Alternatively, comparison of the pressure and imaging data from the homogeneous experiment (i.e., Fig. 3 and the right column of Fig. 4) shows no early heat release or reaction fronts prior to autoignition, and the chemiluminescence at autoignition is spatially uniform. Furthermore, the maximum intensity of the images corresponds exactly with the maximum rate of pressure rise at t = 15.6 ms. Comparing the imaging data at the time of

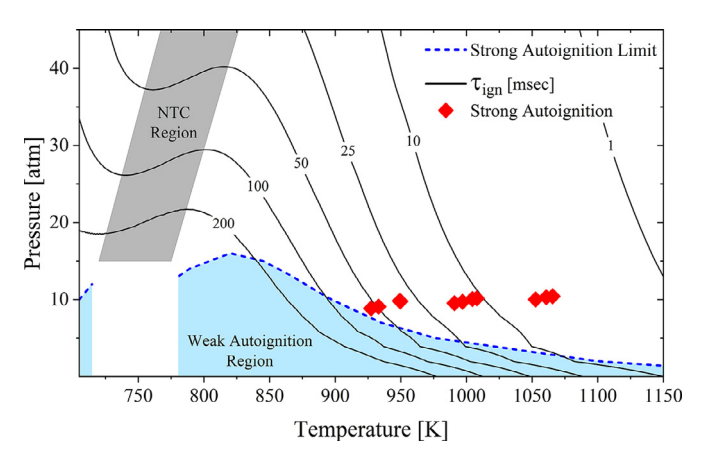


Fig. 5. Experimental results for autoignition regimes for $\phi=0.25$ as a function of state conditions. Calculated autoignition delay time contours, $\tau_{\rm ign}$ [ms], are shown as solid lines. The unshaded region is the strong autoignition regime based on the Sankaran Criterion for the strong autoignition limit assuming a 5 K/mm thermal gradient. The shaded region below the strong autoignition limit (dashed line) denotes the weak autoignition regime. Additionally, the location of the NTC region is highlighted and labeled.

autoignition from the mixed and strong autoignition experiments highlights the non-uniformity of the chemiluminescence caused by the reaction fronts at the mixed autoignition conditions.

The pressure data were used to determine the autoignition delay time and thermodynamic state conditions for each experiment. First the pressure data were filtered using a 75-point smoothing algorithm to reduce noise from the pressure transducer, and the pressure derivative was calculated. The autoignition delay time (τ) was defined as the time from the end-of-compression (i.e., the time of maximum pressure due to compression of the test gas mixture by the sabot) to the time of maximum dP/dt, as shown in Figs 2 and 3. The primary uncertainty in the autoignition delay time is due to the noise in the pressure data, resulting in a maximum uncertainty of \pm 0.6 ms.

The pressure for each experiment was defined as the time-averaged value of pressure from the end-of-compression to the time of maximum dP/dt. The temperature was then defined using isentropic state relations and the actual mixture properties, as described in Donovan et al. [43]. The primary uncertainty in the pressure is due to noise in the transducer data and is assessed as <0.4 atm based on different smoothing algorithms. The uncertainty in temperature is primarily due to propagation of the uncertainty of the pressure measurements, and is estimated as <10 K. A summary of the state conditions and measured autoignition delay times is provided in the Supplemental Material. Alternative methods for assigning state conditions are discussed further below.

3.1. Autoignition behavior

All experiments were identified using the imaging data as either mixed autoignition (where reaction fronts were observed prior to volumetric autoignition) or strong autoignition (where no reaction fronts were observed prior to volumetric autoignition). No experiments exhibited characteristics of weak autoignition (where only reaction fronts consume the reactants with no volumetric autoignition). The results for the classifications of the experiments are presented on pressure-temperature diagrams for $\phi=0.25$ in Fig. 5 and for $\phi=0.5$ in Fig. 6, and the figures include autoignition delay time contours and the strong autoignition limits based on the Sankaran Criterion/Eq. (1). Recall, the autoignition delay time contours and the parameters used to define the strong autoignition limit were calculated using Chemkin modeling and the Healy et al. [45] reaction mechanism. No other propane autoignition studies

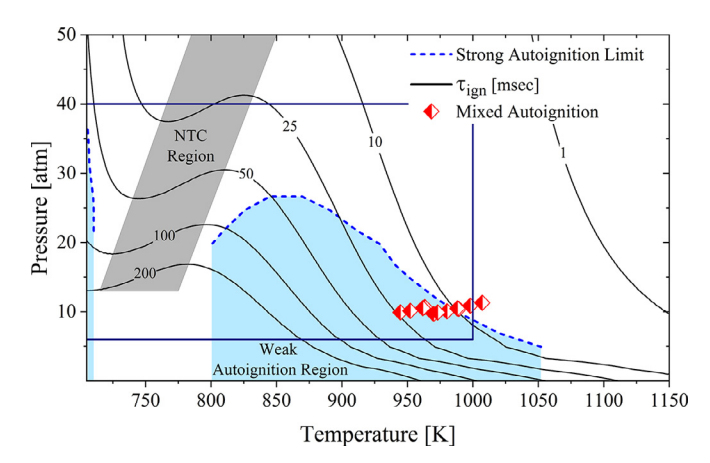


Fig. 6. Experimental results for autoignition regimes for $\phi=0.5$ as a function of state conditions. Calculated autoignition delay time contours, $\tau_{\rm ign}$ [ms], are shown as solid lines. The unshaded region is the strong autoignition regime based on the Sankaran Criterion for the strong autoignition limit assuming a 5 K/mm thermal gradient. The shaded region below the strong autoignition limit (dashed line) denotes the weak autoignition regime. The box indicates the approximate bounds of the experimental conditions of the low-temperature studies presented in Fig. 1. Additionally, the location of the NTC region is highlighted and labeled.

that include imaging data for regime classification are available in the literature. However, the range of conditions considered in previous autoignition studies of propane for $\phi=0.5$ is highlighted in Fig. 6.

The experimental results for $\phi=0.25$ resulted in autoignition delay times from 4 ms to 56 ms in the temperature range of 930–1070 K and the pressure range of 8.9–10.4 atm. The high-speed imaging data indicated spatially uniform autoignition behavior with no flame front propagation prior to autoignition (i.e., strong autoignition) for all $\phi=0.25$ experiments. As seen in Fig. 5, the results are in excellent agreement with expectations based on the Sankaran Criterion for the strong autoignition limit.

Figure 6 presents the autoignition regime classification results for mixtures with $\phi = 0.5$. The autoignition delay times varied from 6 ms to 22 ms in the temperature range of 945 - 1000 K and the pressure range of 9.7-11.3 atm. The high-speed imaging data confirmed the presence of reaction fronts (with pre-ignition heat release) prior to volumetric autoignition for all the $\phi = 0.5$ experiments. The results are generally consistent with expectations based on the Sankaran Criterion, with most of the mixed autoignition experiments falling within the weak autoignition regime. While some of the experimental conditions at higher temperatures might have been expected to yield strong autoignition, the strong autoignition limit plotted in Fig. 6 does not include uncertainty bounds, which might reasonably extend the strong autoignition limit to include the experimental data. Also superimposed on the autoignition regime diagram in Fig. 6 is the approximate range of state conditions of the low-temperature studies presented in the Arrhenius diagram in Fig. 1. The superposition highlights that many of the data from the experimental studies of propane at low temperature may be affected by mixed autoignition characteristics.

3.2. Autoignition delay time

Figures 7 and 8 summarize the autoignition delay time results as a function of inverse temperature for the two equivalence ratios studied in the present work. The error bars represent the uncertainties in the measurements described previously and the uncertainties in the model predictions described in the Supplemental Material. In Figs. 7 and 8, the two panels show the comparison between the experimental measurements and the model predictions where two different methods are used to

define the thermodynamic state conditions of the experiments. Recall, the state conditions of the experiments are also the initial conditions used in the 0-dimensional Chemkin modeling, with the volume and total energy of the system fixed during the simulation, allowing the pressure and temperature to change as the simulated reactions progress. Note that, while localized ignition and propagation of the reaction fronts affect the unburned gases by increasing pressure (and therefore temperature), the 0D homogeneous reactor is still an appropriate first order representation of the system, since mass transport does not occur on a time scale to impact the unburned gases. In Figs. 7(a) and 8(a), the temperature and pressure are based on the time-averaged pressure from the end of compression to the time of maximum pressure rise. As seen in the pressure history data in Fig. 2, this definition includes the effects of pre-autoignition heat release and compression heating of the unburned gases by reaction front propagation. In Figs. 7(b) and 8(b), the temperature and pressure are based on the time-averaged pressure from the end of compression to the time of minimum pressure before autoignition, P_{\min} . This definition neglects pre-autoignition heat release. For strong autoignition conditions, where negligible pre-autoignition heat release was observed, the difference in definitions should have little effect on the experimental and model results, which is consistent with the results shown in Fig. 7. Additionally, the model predictions using the Healy et al. mechanism [45] at the strong $\phi = 0.25$ conditions are in excellent agreement with the experimental measurements.

On the other hand, Fig. 8 shows the impact of mixed autoignition and the associated pre-autoignition heat release on the assigned state conditions and on the comparison between physical measurements and model predictions. As seen in Fig. 8(a), when the effects of early heat release are included in defining the state conditions, the model predictions and experimental data generally agree within the uncertainty limits. However, when preautoignition heat release is neglected, as in Fig. 8(b), the model predictions are systematically higher than the experimental measurements, and the effects are larger at lower temperatures with a maximum discrepancy of a factor of three observed between the experimental results and model predictions. The trend for agreement between model predictions and experimental measurements follows closely with the proximity to the strong autoignition regime (see Fig. 6).

Comparison of the experimental data in the two panels in Fig. 8 also shows reaction fronts can lead to observable effects on the Arrhenius diagram due to differences in the assigned state conditions. Specifically, while the temperature and pressure for an experiment do not impact the measurement of the autoignition delay time from the pressure history data, changing the assigned temperature shifts the data along the x-axis. Additionally, if the autoignition delay time data are scaled based on pressure (as in Fig. 1), changing the assigned pressure shifts the data on the vertical axis of the Arrhenius diagram as well. Depending on the amount of pre-autoignition heat release, using time-averaged state conditions that do or do not include the effects of pre-autoignition heat release can significantly rearrange the data, as most dramatically illustrated by comparing the four lowest temperature data in Fig. 8(a) and (b). In the current work, maximum differences in pressure of 1.0 atm and in temperature of 23 K were determined when the two methods were applied to mixed autoignition experiments, compared with maximum differences of 0.2 atm and 5 K with strong autoignition experiments. Note, some studies use volume histories of compression of an inert gas mixture to model RCM experiments. Such an approach would not capture the effects of reaction fronts and the associated heat release and would be expected to yield systematically higher autoignition delay times.

The experimental autoignition delay time results from the current work are compared with previous autoignition studies of

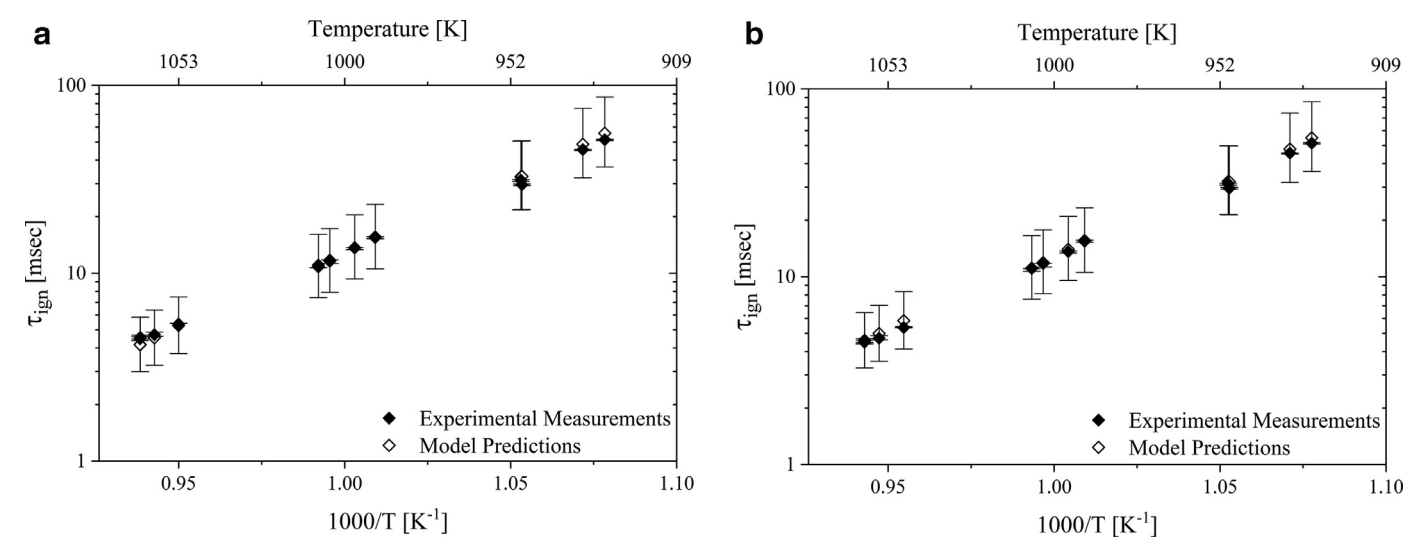


Fig. 7. Measured and predicted autoignition delay times for $\phi = 0.25$ where strong autoignition was observed for all experiments: (a) state conditions based on the time-averaged pressure from the end-of-compression to maximum dP/dt, (b) state conditions based on the time-averaged pressure from the end-of-compression to P_{\min} prior to autoignition. For both panels, the error bars represent the uncertainties of the experimental measurements and model predictions.

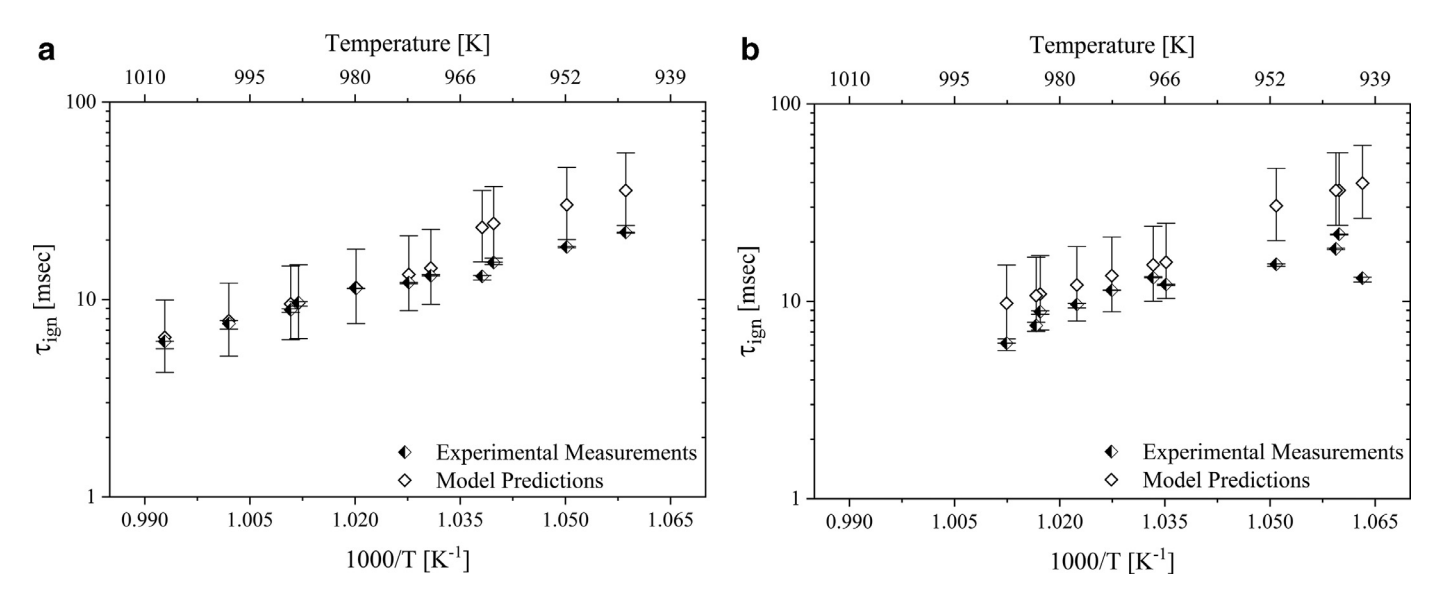


Fig. 8. Measured and predicted autoignition delay times for $\phi = 0.5$ where mixed autoignition was observed for all experiments: (a) state conditions based on the time-averaged pressure from the end-of-compression to maximum dP/dt, (b) state conditions based on the time-averaged pressure from the end-of-compression to P_{\min} prior to autoignition. For both panels, the error bars represent the uncertainties of the experimental measurements and model predictions.

propane at an equivalence ratio of $\phi = 0.5$ in Fig. 9, where all data have been normalized to P=10 atm using scaling of $\tau_{\rm ign} \propto$ 1/P and normalized to air dilution levels using scaling of $\tau_{\rm ign} \propto$ concentration of diluent. In Fig. 9, the state conditions that include the effects of pre-autoignition heat release were used for the UM-RCF data. Also in the figure, the mixture and state conditions reported in the prior studies were used with the Sankaran Criterion (Fig. 6) to categorize the prior experiments as in the weak or strong autoignition regimes. The results of the current work are within the range of values reported previously for au_{ign} at similar conditions; however, comparison of the state conditions used in prior studies with the autoignition diagram of Fig. 6 indicates some of the previous studies were likely in the weak autoignition regime and may have been affected by reaction fronts. Notably, in the temperature region covered in the current work, the scatter in the autoignition delay time data is at least an order of magnitude.

The scatter could be due (in part) to the propagation of localized reaction fronts, and the use of time-integrated pressure data (or other means to account for pre-autoignition heat release) to assign state conditions could possibly correct for some of the scatter (as in Fig. 8). However, the pressure histories of the prior studies are not available for the majority of the data reported in the literature. Model predictions for P=10 atm are also shown in Fig. 9 and are in excellent agreement with the current work and other studies at strong autoignition conditions. Notably, experimental data farthest from the model predictions are in the weak autoignition regime. Also note for P=10 atm, NTC behavior is predicted for temperatures below 800 K and will likely contribute further to the scatter at temperatures below 800 K.

Figure 10 presents a comparison of the current results with prior studies of propane mixtures at $\phi = 0.25$. As with Fig. 9, the data have been scaled to P = 10 atm and air levels of dilution.

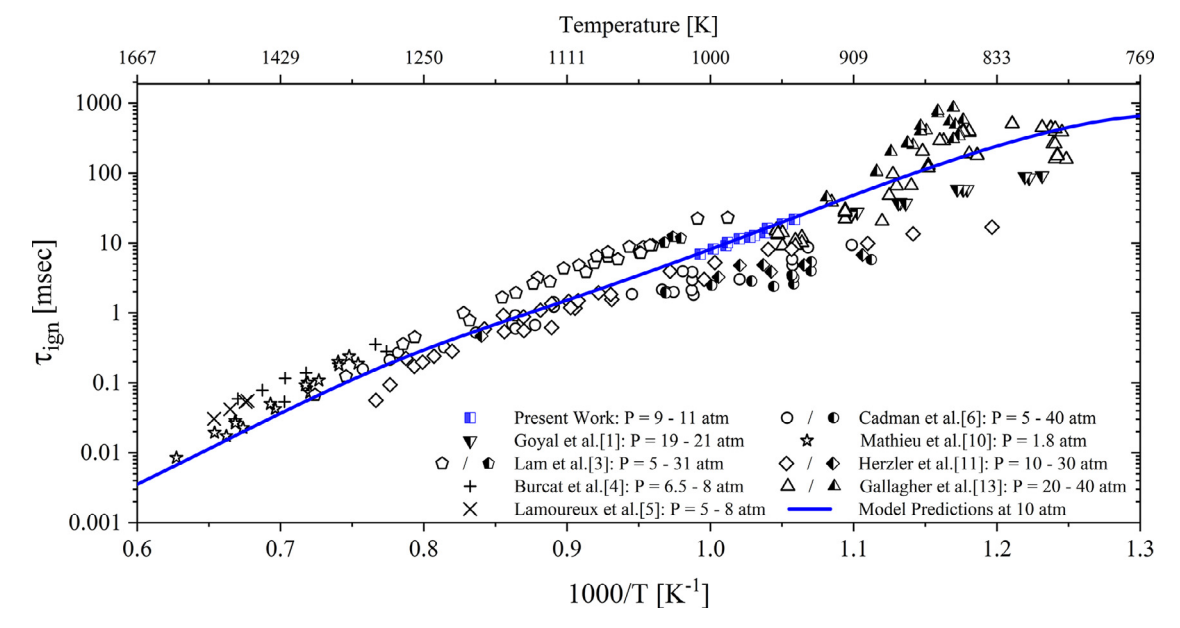


Fig. 9. Comparison of autoignition delay time measurements for propane/air mixtures at ϕ =0.5. All data have been normalized to P = 10 atm and air dilute conditions. Based on the reported state conditions and using the Sankaran Criterion presented in Fig. 6, half-filled symbols are in the weak autoignition region and unfilled symbols are in the strong autoignition region.

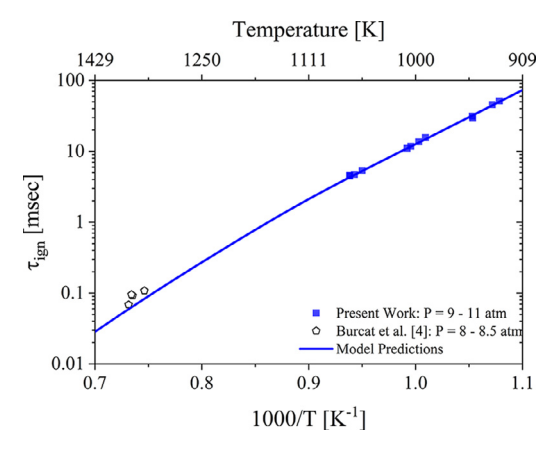


Fig. 10. Comparison of autoignition delay time measurements for propane/air mixtures at ϕ =0.25. All data have been normalized to P = 10 atm and air dilute conditions. Based on the reported state conditions and using the Sankaran Criterion presented in Fig. 6, the filled and unfilled symbols are in the strong autoignition region.

There are no previous studies at low temperatures for propane at $\phi=0.25$; only the current RCF study. All data presented in Fig. 10 are in the strong autoignition region, and model predictions included in Fig. 10 show excellent agreement with both experimental studies.

4. Conclusions

This work provides the first experimental results to categorize the autoignition behavior of propane mixtures using pressure and imaging data simultaneously acquired at low-temperature conditions. Autoignition behavior for lean propane-air mixtures exhibited exclusively strong (spatially homogeneous) autoignition characteristics at the state conditions studied with mixtures of $\phi=0.25$ and exclusively mixed (spatially inhomogeneous with propagation of localized reaction fronts) autoignition characteristics at the state conditions studied with mixtures of $\phi=0.5$. The results supported the validity of the Sankaran Criterion as a

means to identify the strong autoignition limit for propane, where the limit shifted to higher temperatures and pressures as the equivalence ratio was increased. High-speed imaging showed the presence of reaction fronts was associated with pre-autoignition heat release for all inhomogeneous autoignition experiments, and homogeneous autoignition did not exhibit heat release prior to autoignition. Model predictions were in excellent agreement with autoignition delay times measured in the current work when time-averaged values including the effects of pre-autoignition heat release were used. Model predictions over-estimated autoignition delay times determined from mixed autoignition experiments if the effects of pre-autoignition heat release were not considered, especially at lower temperatures.

The results of this study quantified the impact of mixed autoignition phenomena on propane autoignition data at low temperatures, and the importance of assigning state conditions that appropriately capture autoignition behavior within the reactor. The effects of state conditions are particularly important when autoignition data are used to inform and validate chemical kinetic models. The results of the current work identified mixed autoignition phenomena as a potential source of the higher scatter observed in the low-temperature autoignition data for propane.

The results of the current work provide further evidence that the Sankaran Criterion is both a powerful means to improve the quality and understanding of low-temperature autoignition data and a useful method for a prior predictions of autoignition behavior. This outcome has potentially far-reaching implications and impact. The Sankaran Criterion should be applied pro-actively to plan autoignition delay time experiments that isolate strong autoignition conditions, which are then ideally suited for chemical kinetics studies. Alternatively, the Sankaran Criterion can be retroactively applied to interpret autoignition delay time data and pressure histories, particularly when imaging data are not available. In particular, the Sankaran Criterion can be used to revise experimental uncertainties on ignition data that are used for development of reaction chemistry, potentially resolving discrepancies observed in experimental and computational studies at these important low temperature conditions.

Declaration of Competing Interest

None.

Acknowledgments

The authors acknowledge the generous support of the U.S. Department of Energy Basic Energy Sciences, Award Number DE-SC0019184; the National Science Foundation, Award Number 1701343; and the National Science Foundation INTERN program.

Supplementary materials

Supplementary material associated with this article can be found, in the online version, at doi:10.1016/j.combustflame.2020.12.001.

References

- [1] T. Goyal, D. Trivedi, O. Samimi Abianeh, Autoignition and flame spectroscopy of propane mixture in a rapid compression machine, Fuel 233 (2018) 56–67.
- [2] O. Samimi-Abianeh, J.A. Piehl, A. Zyada, M. Al-Sadoon, L. Brave, Effect of diluents on the autoignition of propane mixtures using a rapid compression machine, Energy Fuels 33 (4) (2019) 3529–3538.
- [3] K.-Y. Lam, Z. Hong, D.F. Davidson, R.K. Hanson, Shock tube ignition delay time measurements in propane/O2/argon mixtures at near-constant-volume conditions, Proc. Combust. Inst. 33 (1) (2011) 251–258.
- [4] A. Burcat, A. Lifshitz, K. Scheller, G. Skinner, Shock-tube investigation of ignition in propane-oxygen-argon mixtures, Symp. (Int.) Combust. 13 (1971) 745–755.
- [5] N. Lamoureux, C. Paillard, V. Vaslier, Low hydrocarbon mixtures ignition delay times investigated behind reflected shock waves, Shock Wave 11 (2002) 309–322
- [6] P. Cadman, G. Thomas, P. Butler, The auto-ignition of propane at intermediate temperatures and high pressures, Phys. Chem. Chem. Phys. 2 (2000) 5411–5419
- [7] C.J. Brown, G.O. Thomas, Experimental studies of shock-induced ignition and transition to detonation in ethylene and propane mixtures, Combust. Flame 117 (1999) 861–870.
- [8] K. Kim, K. Shin, Shock Tube and modeling study of the ignition of propane, Bull. Korean Chem. Soc. 22 (2001) 303–307.
- [9] D. Healy, H.J. Curran, S. Dooley, J.M. Simmie, D.M. Kalitan, E.L. Petersen, G. Bourque, Methane/propane mixture oxidation at high pressures and at high, intermediate and low temperatures, Combust. Flame 155 (3) (2008) 451–461.
- [10] O. Mathieu, J. Goulier, F. Gourmel, M.S. Mannan, N. Chaumeix, E.L. Petersen, Experimental study of the effect of CF3I addition on the ignition delay time and laminar flame speed of methane, ethylene, and propane, Proc. Combust. Inst. 33 (3) (2015) 2731–2739.
- [1] J. Herzler, L. Jerig, P. Roth, Shock-tube study of the ignition of propane at intermediate temperatures and high pressures, Combust. Sci. Technol. 176 (10) (2004) 1627–1637
- [12] P. Dagaut, M. Cathonnet, J.C. Boettner, Kinetic modeling of propane oxidation and pyrolysis, Int. J. Chem. Kinet. 24 (1992) 813–837.
- [13] S.M. Gallagher, H.J. Curran, W.K. Metcalfe, D. Healy, J.M. Simmie, G. Bourque, A rapid compression machine study of the oxidation of propane in the negative temperature coefficient regime, Combust. Flame 153 (1/2) (2008) 316–333.
- [4] A. Ramalingam, Y. Fenard, A. Heufer, Ignition delay time and species measurement in a rapid compression machine: a case study on high-pressure oxidation of propane, Combust. Flame 211 (2020) 392–405.
- [5] M. Cathonnet, J.C. Boettner, H. James, Experimental study and numberical modeling of high temperature oxidation of propane and n-butane, Symp. (Int.) Combust. 18 (1981) 903–913.
- [16] D.J. Beerer, V.G. McDonell, An experimental and kinetic study of alkane autoignition at high pressures and intermediate temperatures, Proc. Combust. Inst. 33 (2011) 301–307.
- [17] J.S. Hoffman, W. Lee, T.A. Litzinger, D.A. Santavicca, W.J. Pitz, Oxidation of propane at elevated pressures: experiments and modeling, Combust. Sci. Technol. 77 (1991) 95–125.
- [18] P. Sabia, M. de Joannon, M.L. Lavadera, P. Giudicianni, R. Ragucci, Autoignition delay times of propane mixtures under MILD conditions at atmospheric pressure, Combust. Flame 161 (2014) 3022–3030.

- [9] P. Dagaut, M. Cathonnet, J.C. Boettner, F. Gaillard, Kinetic modeling of propane oxidation, Combust. Sci. Technol. 56 (1987) 23–63.
- [20] S.S. Merchant, C.F. Goldsmith, A.G. Vandeputte, M.P. Burke, S.J. Klippenstein, W.H. Green, Understanding low-temperature first-stage ignition delay: propane, Combust. Flame 161 (10) (2015) 3658–3673.
- [2] S.S. Goldsborough, S. Hochgreb, G. Vanhove, M.S. Wooldridge, H.J. Curran, C.J. Sung, Advances in rapid compression machine studies of low- and intermediate autoignition phenomena, Prog. Energy Combust. Sci. 63 (2017) 1–78.
- [22] G.A. Richards, M.M. McMillian, R.S. Gemmen, W.A. Rogers, S.R. Cully, Issues for low-emission, fuel-flexible power systems, Prog. Energy Combust. Sci 27 (2) (2001) 141–169.
- [23] S. Saxena, I.D. Bedoya, Fundamental phenomena affecting low temperature combustion and HCCI engines, high load limits and strategies for extending these limits, Prog. Energy Combust. Sci. 39 (2013) 457–488.
- [24] X. Lu, D. Han, Z. Huang, Fuel design and management for the control of advanced compression-ignition combustion modes, Prog. Energy Combust. Sci. 37 (2011) 741–783.
- [25] A.B. Mansfield, M.S. Wooldridge, H. Di, X. He, Low-temperature ignition behavior of iso-octane, Fuel 139 (2015) 79–86.
- [26] A.B. Mansfield, M.S. Wooldridge, High-pressure low-temperature ignition behavior of syngas mixtures, Combust. Flame 161 (9) (2014) 2242–2251.
- [27] P. Pal, A.B. Mansfield, P.G. Arias, M.S. Wooldridge, H.G. Im, A computational study of syngas auto-ignition characteristics at high-pressure and low-temperature conditions with thermal inhomogeneities, Combust. Theory Model. 19 (5) (2015) 587–601.
- [28] S.M. Walton, X. He, B.T. Zigler, M.S. Wooldridge, A. Atreya, An experimental investigation of iso-octane ignition phenomena, Combust. Flame 150 (3) (2007) 246–262.
- [29] D. Assanis, S.W. Wagnon, M.S. Wooldridge, An experimental study of flame and autoignition interactions of iso-octane and air mixtures, Combust. Flame 162 (4) (2015) 1214–1224.
- [30] G. Bansal, H.G. Im, Autoignition and front propagation in low temperature combustion engine environments, Combust. Flame 158 (11) (2011) 2105–2112.
- [31] J.W. Meyer, A.K. Oppenheim, On the shock-induced ignition of explosive gases, Symp. (Int.) Combust. 13 (1) (1971) 1153–1164.
- [32] R. Blumenthal, K. Fieweger, K.H. Kom, G. Adomeit, Gas dynamic features of self-ignition of non-diluted fuel/air mixtures at high pressure, Combust. Sci. Technol. 113 (1) (1996) 137–166.
- [33] K. Fieweger, R. Blumenthal, G. Adomeit, Shock-tube investigations on the self-ignition of hydrocarbon-air mixtures at high pressures, Symp. (Int.) Combust. 25 (1) (1994) 1579–1585.
- [34] D.J. Vermeer, J.W. Meyer, A.K. Oppenheim, Auto-ignition of hydrocarbons behind reflected shock waves, Combust. Flame 18 (3) (1972) 327–336.
- [35] K. Fieweger, R. Blumenthal, G. Adomeit, Self-ignition of S.I. engine model fuels: a shock tube investigation at high pressure, Combust. Flame 109 (4) (1997) 599-619.
- [36] J. Shao, R. Choudhary, A.J. Susa, Y. Peng, D.F. Davidson, R.K. Hanson, High-speed imaging of n-heptane ignition in a high-pressure shock tube, Proc. Combust. Inst. (2020), doi:10.1016/j.proci.2020.06.158.
- [37] V.A. Troutman, C.L. Strand, M.F. Cambell, A.M. Tulgestke, V.A. Miller, D.F. Davidson, R.K. Hanson, High-speed OH* chemiluminescence imaging of ignition through a shock tube end-wall, Appl. Phys. B 122 (56) (2016) 1–7.
- [38] D.M.A. Karwat, S.W. Wagnon, M.S. Wooldridge, C.K. Westbrook, Low-temperature speciation and chemical kinetic studies of n-heptane, Combust. Flame 160 (12) (2013) 2693–2706.
- [39] Ya.B. Zeldovich, Regime classification of an exothermic reaction with nonuniform initial conditions, Combust. Flame 39 (2) (1980) 211–214.
- [40] R. Sankaran, H.G. Im, E.R. Hawkes, J.H. Chen, The effects of non-uniform temperature distribution on the ignition of a lean homogeneous hydrogen-air mixture, Proc. Combust. Inst. 30 (1) (2005) 875–882.
- [41] H.G. Im, P. Pal, M.S. Wooldridge, A.B. Mansfield, A regime diagram for autoignition of homogeneous reactant mixtures with turbulent velocity and temperature fluctuations, Combust. Sci. Technol. 187 (2015) 1263–1275.
- [42] K.P. Grogan, S.S. Goldsborough, M. Ihme, Ignition regimes in rapid compression machines, Combust. Flame 162 (8) (2015) 3071–3080.
- [43] M.T. Donovan, X. He, B.T. Zigler, T.R. Palmer, M.S. Wooldridge, A. Atreya, Demonstration of a free-piston rapid compression facility for the study of high temperature combustion phenomena, Combust. Flame 137 (3) (2004) 351–365.
- [44] X. He, B.T. Zigler, S.M. Walton, M.S. Wooldridge, A. Atreya, A rapid compression facility study of OH time histories during iso-octane ignition, Combust. Flame 145 (3) (2006) 552–570.
- [45] D. Healy, D.M. Kalitan, C.J. Aul, E.L. Petersen, G. Bourque, H.J. Curran, Oxidation of C1–C5 alkane quinternary natural gas mixtures at high pressures, Energy Fuels 24 (3) (2010) 1521–1528.
- [46] CHEMKIN-PRO 15112, Reaction design: San Diego, 2011.